Electronic Supplementary Information

Ion Conduction in the Comb-branched Polyether Electrolytes with Controlled Network Structures

Lu Xu,[†,‡] Wei Wei,[†,‡] Donglei You,[†] Huiming Xiong[†,*] and Jun Yang[§]

[†]Department of Polymer Science, [§]Shanghai Electrochemical Energy Devices Research Center, School of Chemistry and Chemical Engineering; Shanghai Jiao Tong University, Shanghai 200240, P. R. China.

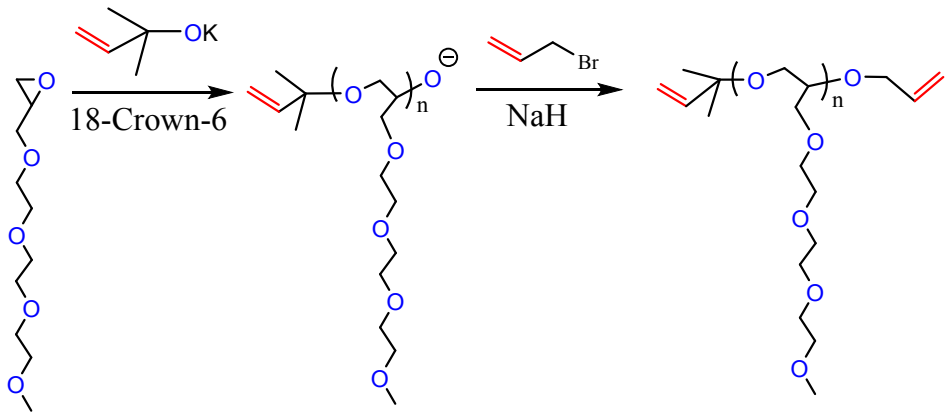

Scheme S1. Synthetic route of end-functionalized PEO^{B} homopolymers.

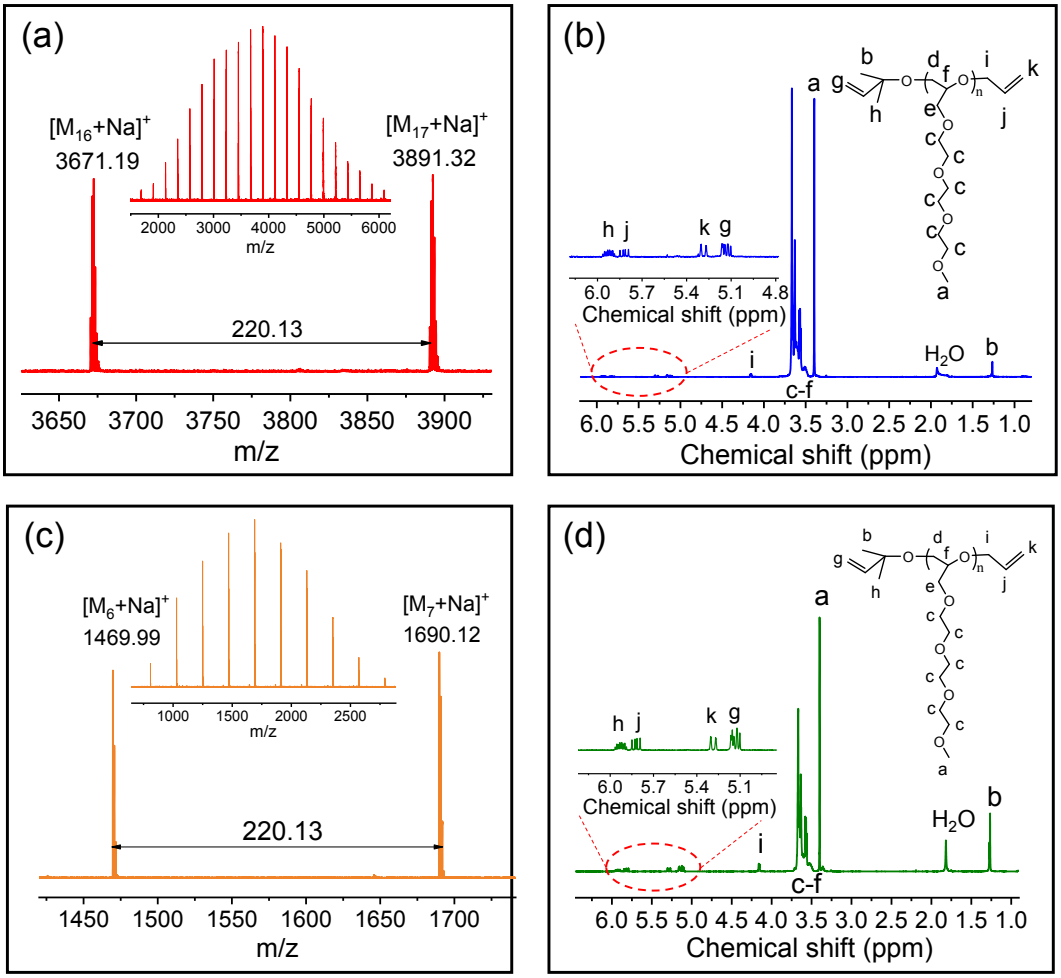

Figure S1. (a) MALDI-TOF mass spectra of end-functionalized homopolymer $PEO^{B}4k$. The inset shows the full spectrum. $[M_{16} + Na]^+$ represents C_5H_9O - $(C_{10}H_{20}O_5)_{16}$ - C_3H_5 - Na^+ and $[M_{17} + Na]^+$ represents C_5H_9O - $(C_{10}H_{20}O_5)_{17}$ - C_3H_5 - Na^+, respectively. (b) ^{1}H-NMR spectra of $PEO^{B}4k$. (c) MALDI-TOF mass spectra of end-functionalized homopolymer $PEO^{B}1.4k$. The inset shows the full spectrum. $[M_6 + Na]^+$ represents C_5H_9O - $(C_{10}H_{20}O_5)_6$ - C_3H_5 - Na^+ and $[M_7 + Na]^+$ represents C_5H_9O - $(C_{10}H_{20}O_5)_7$ - C_3H_5 - Na^+, respectively. (d) ^{1}H-NMR spectra of $PEO^{B}1.4k$.

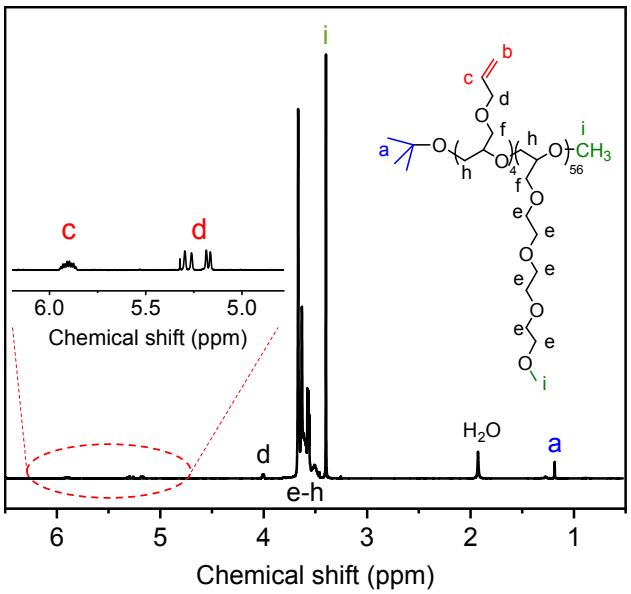

Figure S2. ^{1}H-NMR spectra of V_4E_{56}. The insert corresponds the enlarged spectrum in range of 4.7~6.3 ppm.

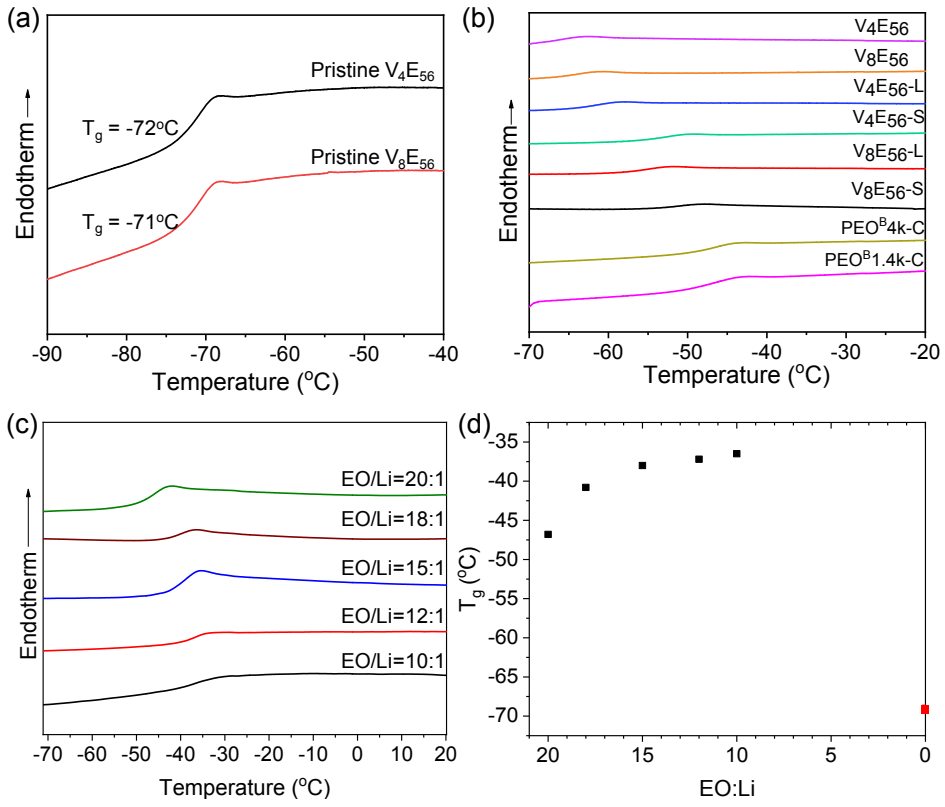

Figure S3. (a) The DSC thermogram of the pristine copolymers during the heating process at the scanning rate of 5 °C/min. (b) The DSC thermogram of the copolymers and the crosslinked SPEs with LiTFSI salt loading of EO/Li=20 during the heating process at the scanning rate of 5 °C/min. (c) The DSC thermogram of the representative PEO^B based SPE with different salt loading during the heating process. (d) The T_g of the SPE as a function of mole ratio between EO units and lithium ion (EO/Li).

DSC experiments were utilized to explore the thermal behaviors of the polymers and the resulting SPEs, as shown in Figure S3. The pristine linear polymers exhibit glass transition temperatures (T_gs) around -72 °C (Figure S3a). No melting transition was observed, suggesting the amorphous nature of the system. With the addition of lithium salt, the T_gs of the polymer/salt blends increase up to ~ -65 °C, as illustrated in Figure S3b. For the crosslinked SPEs, the T_gs are generally 10 °C higher than that of the pristine linear polymers. In addition, the T_gs show slight dependence on the crosslink density in the SPEs. The V_8E_{56}-S and V_8E_{56}-L SPEs with higher crosslink densities possess typically higher T_gs compared with that of the V_4E_{56}-S and V_4E_{56}-L samples. Among the four elastomers herein, the V_8E_{56}-S with the smallest mesh size exhibits the highest T_g of -52 °C. For end-crosslinked PEO^B system, T_gs are around -48 °C, which are higher than side-crosslinked copolymer system, indicating a denser network structure. The influence of the salt loading on the T_gs of SPE is characterized by DSC, as shown in Figure S3c and S3d. Upon increasing the salt concentration in the elastomer, the T_gs of the SPE are found to gradually increase from -71 °C to -37 °C (Figure S3d), ascribed to the increase of Li-EO interactions. The detailed thermal properties of the SPEs are summarized in Table 1. The nanostructures of the SPEs were further identified by the WAXD experiments. The WAXD profiles of the crosslinked samples shown in Figure S4 exhibit the diffused halo in the wide angel region (q~15.5 nm^{-1}), indicating amorphous state of the SPEs. In contrast, the linear PEO displays multiple sharp scattering in the X-ray profile, attributed to the crystalline nature of the sample. The intrinsic non-crystalline properties of the SPEs are expected to impart the system preeminent ability to lithium ion transport.

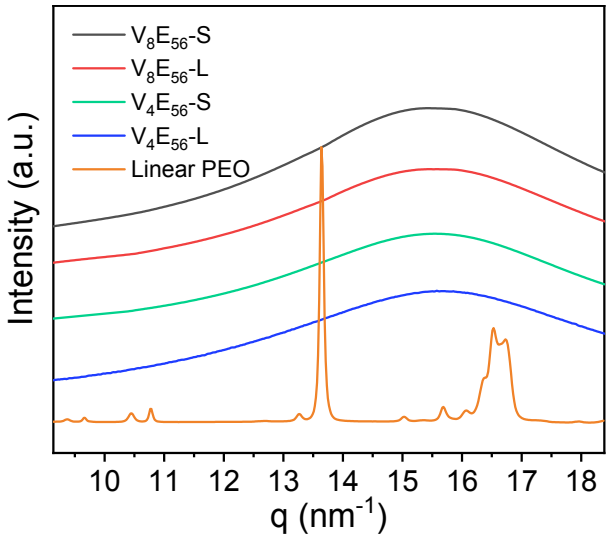

Figure S4. WAXD profiles of the SPEs and linear PEO at room temperature.

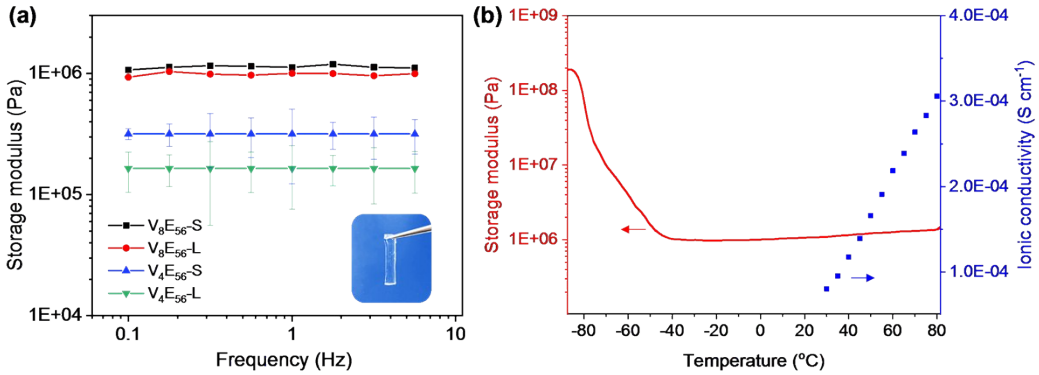

Figure S5. (a) Storage moduli of the SPEs at 30 °C and different frequency derived from the DMA measurements. The inset corresponds to the photograph of the typical SPE film. (b) Temperature-dependent storage modulus and ionic conductivity of the representative SPE of V_8E_{56}-S. The storage modulus was collected at 1 Hz in the DMA test.

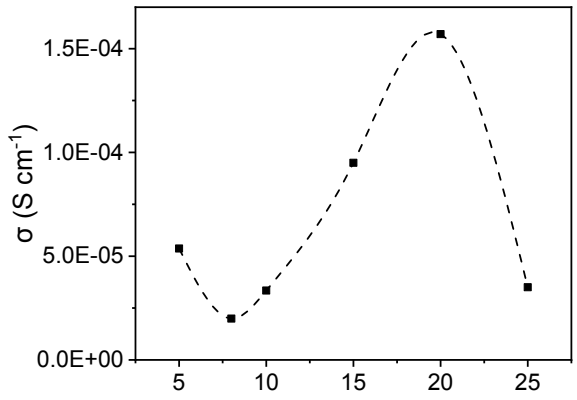

Figure S6. Relationship between salt concentration and ionic conductivity in V_4E_{56}-L.

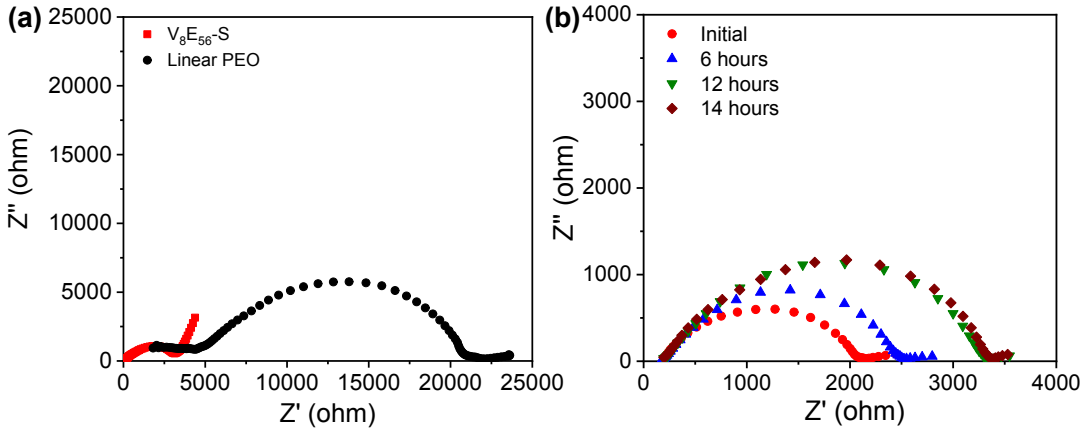

Figure S7. (a) Typical EIS profiles of Li/V_8E_{56}-S/Li and Li/linear PEO/Li cells at 30 ^oC. The inset is the enlarged view of the EIS curve of V_8E_{56}-S. (b) Time dependent impedance spectra of Li/V_8E_{56}-S/Li cell at 30 ^oC. The interfacial resistance was found to slightly increase initially and become stable after 12 hours of storage.

Table S1. Comparison of ionic conductivity of V_xE_y based SPEs with PEO systems reported in literatures.

Sample	σ at 30 ^oC (S cm^{-1})	σ at 60 ^oC (S cm^{-1})	Ref.
V_4E_{56}-L	1.6E-4	4.8E-4	This work
PEO-SiO_2	4.4E-5	1.2E-3	[1]
4PEG2K-POSS	4.4E-5	2.2E-4	[2]
DN PEO	3.2E-5	5.0E-4	[3]
PEO-Garnet	1.0E-4	6.3E-4	[4]
PEO network	4.0E-6	1.0E-4	[5]
PEO+LLZO	1.1E-4	2.5E-4	[6]
PEO+LGPS	2.5E-5	7.9E-4	[7]

Table S2. Characteristic IR vibrational bands of lithium containing SPEs.

	$\nu_s(CH_2)$	$\delta(CH)$	$\nu_s(C\text{-}O\text{-}C)$	$\nu_a(SO_2)$	$\nu_s(SO_2)$	$\nu_a(CF_3)$	$\nu(S\text{-}N)$
Wavenumber (cm^{-1})	2875	1455	1056	1334, 1350	1136	1193	739

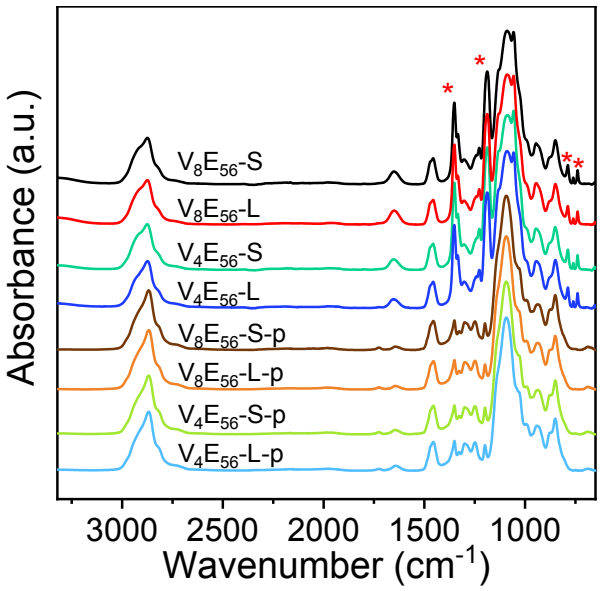

Figure S8. (a) FT-IR absorption spectra of SPEs with LiTFSI and pristine film without salt (denoted as V_xE_y-S-p or V_xE_y-L-p). Asterisks are the characteristic bands of LiTFSI.

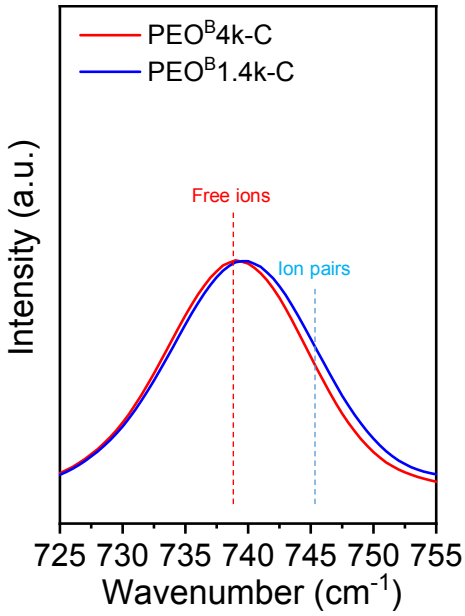

Figure S9. Raman spectra for end-crosslinked PEO^B SPEs with LiTFSI in the 755-725 cm^{-1} wavenumber region.

Author Contributions

‡These authors contributed equally.

Reference:

1 D. C. Lin, W. Liu, Y. Y. Liu, H. R. Lee, P. C. Hsu, K. Liu and Y. Cui, *Nano Lett.*, 2016, **16**, 459-465.

2 Q. W. Pan, D. M. Smith, H. Qi, S. J. Wang and C. Y. Li, *Adv. Mater.*, 2015, **27**, 5995-6001.

3 H. Duan, Y. X. Yin, X. X. Zeng, J. Y. Li, J. L. Shi, Y. Shi, R. Wen, Y. G. Guo and L. J. Wan, *Energy Storage Materials*, 2018, **10**, 85-91.
4 L. Chen, Y. Li, S. P. Li, L. Z. Fan, C. W. Nan and J. B. Goodenough, *Nano Energy*, 2018, **46**, 176-184.
5 H. Ben youcef, O. Garcia-Calvo, N. Lago, S. Devaraj and M. Armand, *Electrochimica Acta*, 2016, **220**, 587-594.
6 H. Xie, C. P. Yang, B. Y. Liu, S. Wang and L. B. Hu, *Adv. Energy Mater.*, 2018, **8**, 1703474.
7 Y. R. Zhao, C. Wu, G. Peng, X. T. Chen, X. Y. Yao, Y. Bai, F. Wu, S. J. Chen and X. X. Xu, *Journal of Power Sources*, 2016, **301**, 47-53.